

Extended gas in Seyfert galaxies: Near infrared observations of NGC 2110 and Circinus

Thaisa Storchi-Bergmann¹*, Cláudia Winge^{1,2}*, Martin J. Ward³ and Andrew S. Wilson^{4,2}

¹ Instituto de Física, UFRGS, Campus do Vale, C.P. 15051, P. Alegre, RS, BRAZIL

² Space Telescope Science Institute, 3700 San Martin Drive, Baltimore, MD 21218, USA

³ Dept. of Physics and Astronomy, University of Leicester, University Road, Leicester LE1 7RH, England

⁴ Astronomy Department, University of Maryland, College Park, MD 20742, USA

14 June 2021

ABSTRACT

We present results of near-IR long-slit spectroscopy in the J and K bands of the Seyfert 2 galaxies NGC 2110 and Circinus. Our goal is to investigate the gaseous distribution, excitation, reddening and kinematics, looking for signatures of the molecular torus hypothesised in unified models to both obscure and collimate the nuclear radiation. The two galaxies show extended emission in the IR emission lines $[\text{Fe II}]\lambda 1.257\mu\text{m}$, $\text{Pa}\beta$ and $\text{H}_2v=1-0\text{ S}(1)$, both along the major axis of the galaxy disk and perpendicular to it. In NGC 2110, the emission line ratio $[\text{Fe II}]/\text{Pa}\beta$ increases towards the nucleus, where its value is ≈ 7 . Further, the nuclear $[\text{Fe II}]$ and $\text{Pa}\beta$ lines are broader ($\text{FWHM} \approx 500 \text{ km s}^{-1}$) than the H_2 line ($\text{FWHM} \leq 300 \text{ km s}^{-1}$). Both these results suggest that shocks, driven by the radio jet, are an important source of excitation of $[\text{Fe II}]$, while the H_2 excitation is dominated by X-rays from the nucleus. $\text{Br}\gamma$ is only observed at the nucleus, where $\text{H}_2/\text{Br}\gamma \approx 3$. In the case of Circinus, both $[\text{Fe II}]/\text{Pa}\beta$ and $\text{H}_2/\text{Br}\gamma$ decrease from ≈ 2 at $4''$ from the nucleus to nuclear values of ≈ 0.6 and ≈ 1 , respectively, suggesting that the starburst dominates the nuclear excitation, while the AGN dominates the excitation further out ($r \geq 2''$). For both galaxies, the gaseous kinematics are consistent with circular rotation in the plane of the disk. Our rotation curves suggest that the nucleus (identified with the peak of the IR continuum) is displaced from the kinematic centre of the galaxies. This effect has been observed previously in NGC 2110 based on the kinematics of optical emission lines, but the displacement is smaller in the infrared, suggesting the effect is related to obscuration. The continuum J–K colours indicate a red stellar population in NGC 2110 and a reddened young stellar population in Circinus, outside the nucleus. Right at the nucleus of both galaxies, the colours are redder, apparently a result of hot dust emission, perhaps from the inner edge of a circumnuclear torus. In NGC 2110, the signature of the hot dust emission is particularly clear in the K-band, being seen as an additional component superimposed on the continuum observed in the J-band.

Key words: galaxies: active – infrared: galaxies – galaxies: ISM – galaxies: individual: NGC 2110 – galaxies: individual: Circinus

1 INTRODUCTION

The nuclear regions of Seyfert 2 galaxies are dusty environments, as revealed by red nuclear colours in optical imag-

* Visiting Astronomer at the Cerro Tololo Interamerican Observatory, operated by the Association of Universities for Research in Astronomy, Inc. under contract with the National Science Foundation.

ing and large Balmer emission-line ratios in spectroscopic studies (e.g. Ward et al. 1987; Storchi-Bergmann, Wilson & Baldwin 1992; Mulchaey et al. 1994, Storchi-Bergmann, Kinney & Challis 1995; Simpson et al. 1996; Cid-Fernandes, Storchi-Bergmann & Schmitt 1998). Although such reddening may be due to large scale dust in the central regions of the host galaxies, dust on smaller scales is believed to be concentrated in an optically thick molecular torus with dimensions of tens of parsecs and surrounding the nuclear

engine (e.g. Antonucci & Miller 1985; Antonucci 1993). This torus both obscures the nucleus from direct view and collimates the ionizing radiation, giving origin to the “ionization cones” observed in Seyfert 2 galaxies (e.g. Mulchaey, Wilson & Tsvetanov 1996). Evidence for reradiation from hot dust emitting in the near-IR has been found, among others, by McAlary & Rieke (1988); Sanders et al. (1989); and Alonso-Herrero, Ward & Kotilainen (1996).

In order to penetrate the dust layers in Seyfert 2 galaxies, it is necessary to observe in the infrared region of the spectrum. At $\lambda \approx 2\mu\text{m}$, $A_K \approx A_V/10$, so near-IR observations can reach deeper into the nuclear region than optical observations. In addition, if there is warm molecular hydrogen near the nucleus, emission from the vibration-rotational transitions of molecular hydrogen (such as $\text{H}_2 v=1-0 \text{ S}(1)$ at rest wavelength $2.122\mu\text{m}$) should be strong. If an H_2 -emitting disc-like structure could be detected elongated perpendicular to the ionization cone or radio axis, this would provide very strong support for the unified model. Narrow-band imaging studies by Blietz *et al.* (1994) have indeed shown that in NGC 1068 the H_2 line emission is spatially extended almost perpendicular to the cone. Similar results have been found for NGC 4945 (Moorwood *et al.* 1996).

With these issues in mind, we have obtained long-slit spectra in the J and K-bands of a number of Seyferts with anisotropic high-excitation optical emission, which, in the unified model, is a result of ionization and excitation by nuclear radiation collimated by the torus. We present in this work the results for NGC 2110 and Circinus, the two galaxies for which we were able to detect IR emission lines at the largest distances from the nuclei.

NGC 2110 is an early-type Seyfert 2 galaxy discovered through its X-ray emission (Bradt *et al.* 1978). Narrow-band images show high excitation gas extending up to $10''$ from the nucleus (Wilson, Baldwin & Ulvestad 1985; Mulchaey *et al.* 1994), in a similar direction to a jet-like radio source at position angle (p.a.) 10° (Ulvestad & Wilson 1983). Wilson & Baldwin (1985) and Wilson, Baldwin & Ulvestad (1985), using optical long-slit spectroscopy, have found extended ionized gas in normal rotation about the photometric minor axis, but with the kinematic centre displaced $\approx 1.7''$ south of the optical continuum nucleus. Adopting a distance to NGC 2110 of 31.2 Mpc (using the systemic velocity from Wilson & Baldwin 1985, for $H_0 = 75 \text{ km s}^{-1}$), we obtain a scale of $151 \text{ pc arcsec}^{-1}$.

The Circinus galaxy is a nearby (~ 4 Mpc) spiral (Freeman *et al.* 1977) with a nuclear spectrum characteristic of both starburst and Seyfert activity (Moorwood & Oliva 1988, 1990). It contains the closest known ionization cone and a circumnuclear starburst ring (Marconi *et al.* 1994). It is a strong H_2O megamaser emitter, and shows radio lobes approximately orthogonal to the galactic plane (Elmoutie *et al.* 1995). Maiolino *et al.* (1998) present H and K images of the inner $13'' \times 13''$, narrow-band images of the central $5'' \times 5''$ and a study of the stellar kinematics using near-IR absorption bands. Davies *et al.* (1998) present narrow-band images in $[\text{Fe II}]\lambda 1.64\mu\text{m}$ and $\text{H}_2 v=1-0 \text{ S}(1)$, as well as radio continuum maps at 3 and 6 cm. Our adopted distance of 4 Mpc (Freeman *et al.* 1977) corresponds to a scale of $19 \text{ pc arcsec}^{-1}$.

2 OBSERVATIONS

Long-slit spectra of NGC 2110 and Circinus in the J and K bands were obtained using the Infrared Spectrograph (IRS) on the 4m telescope of the Cerro Tololo Interamerican Observatory in the nights of Nov. 1 and 2, 1995 and March 2, 1996. The scale of the 256×256 InSb detector was $0.363''$ per pixel, and the useful slit length was $15''$. Two gratings were used: one with 75 lines per mm, and resolution $R \approx 700$ (~ 4 pixels), hereafter LR grating, and the other with 210 lines per mm, and $R \approx 2000$, hereafter HR grating. The corresponding velocity resolutions are $\approx 400 \text{ km s}^{-1}$ and 150 km s^{-1} , respectively. The slit width was either $1.1''$ or $1.7''$, depending on the seeing.

NGC 2110 was observed along two position angles: p.a. = 170° , which is close to both the major axis of the inner isophotes in the narrow-band [OIII] image of Mulchaey *et al.* (1994) and the major axis of the galaxy disk, and along the perpendicular direction, at p.a. = 80° . Circinus was observed along the approximate axis of the radio lobes in p.a. = -66° , and along the approximate galaxy major axis in p.a. = 24° . A log of the observations is presented in Table 1.

Wavelength calibrations in the J and K bands were obtained using an He Ar lamp and OH sky lines, respectively. The reduction was performed using IRAF through scripts kindly made available by Richard Elston (available at the CTIO ftp archive). One-dimensional spectra were extracted binning together 2 pixels ($0.73''$), except for the outermost locations where 4 pixels ($1.46''$) were co-added to improve the signal to noise ratio (S/N). The atmospheric absorption features were removed using spectra of nearby stars bracketing the galaxy observations; each extracted spectrum was divided by the normalized spectrum of a star (or the average between the spectra of two stars, one observed before and the other after the galaxy). The spectra were then flux calibrated using observations of standard stars from Elias *et al.* (1982).

3 RESULTS

3.1 NGC 2110

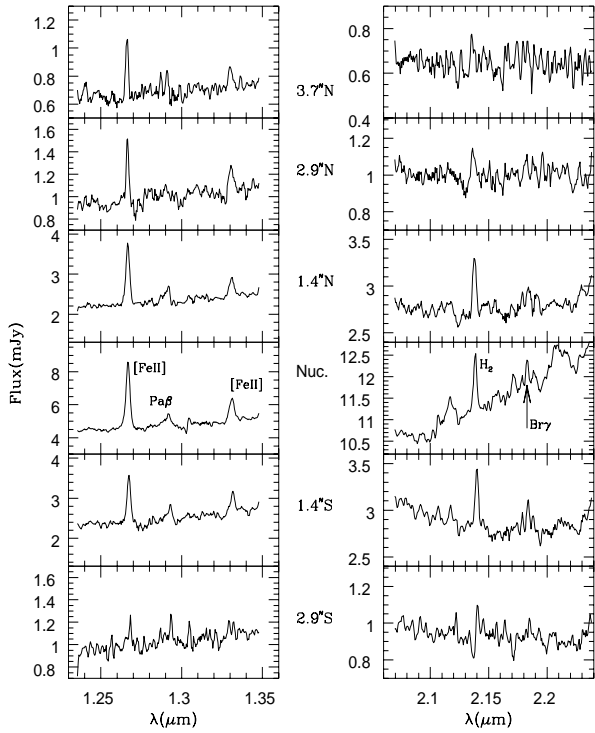
3.1.1 Emission-line Profiles

Sequences of J and K-band spectra obtained with the LR grating are presented in Figs. 1 (p.a. = 170°) and 2 (p.a. = 80°). The higher dispersion spectra obtained with the HR grating are shown in Fig. 3. The strongest emission line in the J-band is $[\text{Fe II}]\lambda 1.257\mu\text{m}$, followed by $[\text{Fe II}]\lambda 1.321$ and $\text{Pa}\beta$. The profiles of $[\text{Fe II}]\lambda 1.257$ and $\text{Pa}\beta$ are better defined in the higher dispersion spectrum of Fig. 3. We find that $\text{Pa}\beta$ is blended with $[\text{Fe II}]\lambda 1.279\mu\text{m}$, which has a predicted flux of 7% that of $[\text{Fe II}]\lambda 1.257\mu\text{m}$. Although the profile of $[\text{Fe II}]\lambda 1.279\mu\text{m}$ is not well defined (due to its low S/N), its full width at half maximum (FWHM) is similar to that of $[\text{Fe II}]\lambda 1.257\mu\text{m}$, and the observed wavelength and flux agree with the expected values.

$[\text{Fe II}]\lambda 1.257\mu\text{m}$ emission is observed up to $\approx 5''$ to the N and $\approx 3''$ to the S, being stronger to N, where both the radio (Ulvestad & Wilson 1983) and optical high-excitation line ([OIII]) emission are stronger (Wilson, Baldwin & Ulvestad 1985; Mulchaey *et al.* 1994).

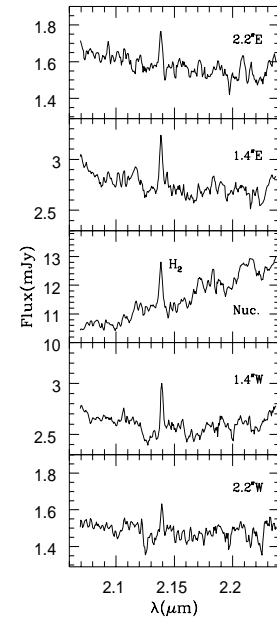
Table 1. Log of Observations

Object	Date	P.A.(°)	Band (μm)	Grating	Exp.Time (sec)	Slit width(‘‘)
NGC 2110	1 November 1995	170	J(1.24-1.35)	75 l/mm	2400	1.1
	2 November 1995	80	K(2.07-2.24)	75 l/mm	2160	1.1
	2 November 1995	170	K(2.07-2.24)	75 l/mm	1800	1.1
	2 March 1996	170	J(1.26-1.30)	210 l/mm	1800	1.7
Circinus	2 March 1996	24	J(1.24-1.29)	210 l/mm	1800	1.7
	2 March 1996	-66	J(1.24-1.29)	210 l/mm	800	1.7
	2 March 1996	-66	K(2.12-2.18)	210 l/mm	800	1.7
	2 March 1996	24	K(2.12-2.18)	210 l/mm	800	1.7

**Figure 1.** J and K-band spectra of NGC 2110 at $R \approx 700$ along the radio axis at $\text{p.a.} = 170^\circ$, after binning 2 pixels ($0.73''$) together. The distance from the nucleus is indicated.

In the K-band, $\text{H}_2 v=1-0 \text{ S}(1)$ is clearly detected to approximately $4''$ N and S and $3''$ E and W of the nucleus (Figs. 1 and 2). $\text{Br}\gamma$ is detected at the nucleus and at $1.4''$ S, but the galaxy continuum is very strong and has a lot of structure, resulting in a large uncertainty for the $\text{Br}\gamma$ flux.

Our nuclear emission-line spectra in the J and K bands are similar to those of Veilleux, Goodrich & Hill (1997), which were obtained with a much larger aperture ($3'' \times 3''$). The difference in aperture size may be responsible for the difference in the K-band continuum, which is much redder in our data. An unresolved, very red nucleus is also found in the HST optical continuum colour map of Mulchaey et al. (1994). Veilleux et al. (1997) report a ratio between the narrow $\text{Br}\gamma$ and H_2 fluxes of ≈ 0.25 , as compared with ≈ 0.35 in our case. They also say they may have detected broad components to $\text{Pa}\beta$ and $\text{Br}\gamma$; the structure in the contin-

**Figure 2.** K-band spectra of NGC 2110 at $R \approx 700$ along $\text{p.a.} = 80^\circ$ (perpendicular to the radio axis), after binning 2 pixels ($0.73''$) together. The distance from the nucleus is indicated.

uum around $\text{Br}\gamma$ precludes any attempt to measure such a component in our spectra.

In Fig. 4 we show a comparison of the line profiles. The top panels show the scaled profiles from the spectra obtained with the HR grating. From the top left panel, it can be seen that the nuclear $\text{Pa}\beta$ profile is very similar to that of the $[\text{FeII}]\lambda 1.257\mu\text{m}$ line, although the blue wing of $\text{Pa}\beta$ is contaminated by $[\text{FeII}]\lambda 1.279\mu\text{m}$, as described above. We do not find evidence in our data for the broad component suspected by Veilleux et al. (1997) in $\text{Pa}\beta$. As our data seems to have similar S/N ratio to theirs, one possibility is that contamination of the blue wing of $\text{Pa}\beta$ by the adjacent $[\text{FeII}]$ line may have been interpreted as a broad component.

Also in Fig. 4, the $[\text{FeII}]$ and $\text{Pa}\beta$ profiles are compared with that of a HeAr (calibration lamp) line, which has $\text{FWHM} = 150 \pm 5 \text{ km s}^{-1}$. Although the signal-to-noise ratio is much lower for $\text{Pa}\beta$, it can be seen that both lines are much broader than the instrumental profile. The FWHM (corrected for the instrumental FWHM above) are

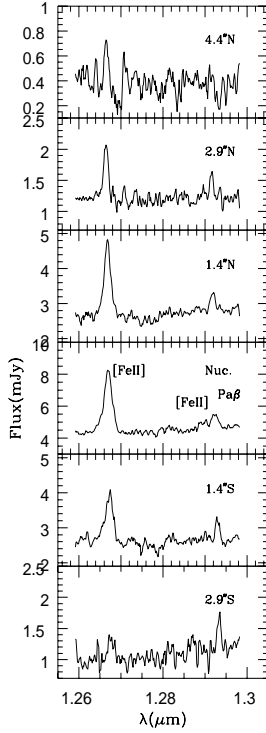


Figure 3. J-band spectra of NGC 2110 at $R \approx 2000$ along the radio axis at $p.a. = 170^\circ$, after binning 2 pixels ($0.73''$) together. The distance from the nucleus is indicated.

520 ± 20 km s $^{-1}$ for [Fe II] and 430 ± 70 km s $^{-1}$ for Pa β . The blue and red wings of the [Fe II] line reach ≈ -900 km s $^{-1}$, and ≈ 600 km s $^{-1}$ at zero intensity, respectively. The [Fe II] profile gets narrower with increasing distance from the nucleus (top right panel of Fig. 4), reaching a corrected FWHM = 240 ± 40 km s $^{-1}$ at $2.9''$ N of the nucleus.

The bottom panels of Fig. 4 show the profiles from the spectra obtained with the LR grating, where it can be seen that the nuclear [Fe II] profile is still resolved. The similarity of the Pa β and [Fe II] profiles is confirmed by these data. The corrected FWHM's of [Fe II] and Pa β are, respectively, 500 ± 40 km s $^{-1}$ and 550 ± 120 km s $^{-1}$, consistent with the values from the higher resolution spectrum. On the other hand, the nuclear H $_2$ profile is barely resolved, being very similar to the profiles of the Pa β and Br γ lines of the planetary nebula NGC 7009, observed as a reference, and which have observed (uncorrected) FWHM ≈ 400 km s $^{-1}$. Correcting the FWHM of the nuclear H $_2$ line for the instrumental profile (adopted as that of the Br γ line of NGC 7009), the resulting FWHM is 230 ± 70 km s $^{-1}$. Finally, in the bottom right panel of Fig. 4 we present the profiles of the H $_2$ line as a function of distance from the nucleus, which show a marginal decrease of FWHM with increasing distance from the nucleus.

We can thus conclude that, at the nucleus of NGC 2110, the [Fe II] and H $_2$ lines originate in different material, the former line coming from more kinematically disturbed gas. The larger widths of the [Fe II] line could result from acceleration of interstellar gas by the radio jet, which might also be responsible for ionizing the species through the agency of shock waves (see section 3.1.3).

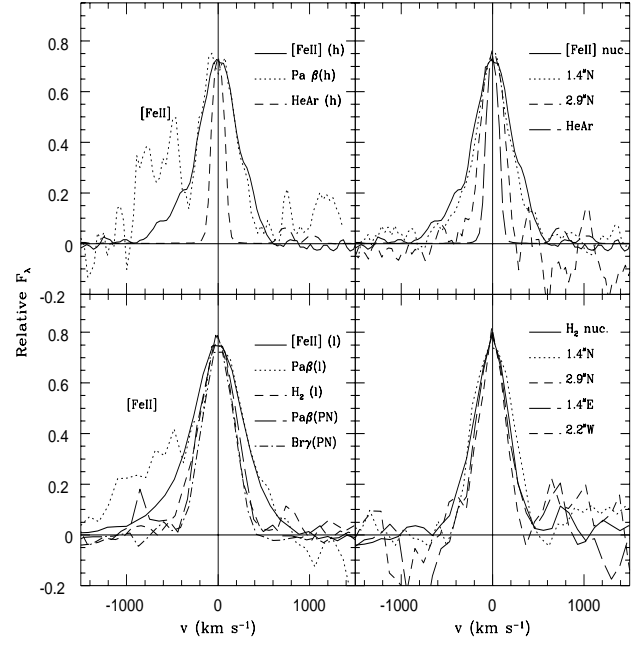


Figure 4. Comparison of the emission-line profiles of NGC 2110. The upper panels correspond to the HR grating and the lower panels to the LR grating. *Upper left:* The nuclear [Fe II] $\lambda 1.257\mu\text{m}$ line profile (continuous line) is compared with that of Pa β (dotted line), as well as with the instrumental profile (dashed line). *Upper right:* A comparison of the [Fe II] $\lambda 1.257\mu\text{m}$ line profiles at different distances from the nucleus along the radio axis. *Bottom left:* Comparison of the nuclear emission-line profiles with those of the planetary nebula NGC 7009, which are representative of the instrumental resolution. *Bottom right:* comparison of the H $_2$ profiles as a function of distance from the nucleus.

3.1.2 Velocity field

Fig. 5 shows the heliocentric velocities derived from the peak wavelengths of the [Fe II] $\lambda 1.257\mu\text{m}$, Pa β and H $_2$ emission lines, from both the LR and HR data. The lower panel shows the velocities along the radio axis at $p.a. = 170^\circ$, for all the emission lines, and the upper panel shows the velocities along $p.a. = 80^\circ$, available only for H $_2$. The good agreement between the velocities derived for [Fe II] using two different gratings gives us confidence in the reliability of the data. For clarity, error bars have not been plotted in the lower panel (the sizes are similar to those in the upper panel). The adopted position of the nucleus corresponds to the peak of the continuum light in the J and K bands.

There is a small difference between the kinematics of the gas emitting [Fe II] and that emitting Pa β and H $_2$: the latter two emission lines show a rotation curve well represented by a circular rotation model (see below), while the [Fe II] rotation curve shows a shallower gradient near the nucleus. Although small, this difference seems to be significant (as compared with the error bars in Fig. 5) and may be related to interaction of the [Fe II] emitting gas with the radio jet, already suggested by the broadening of its emission line profile.

It is interesting to compare the near-IR and optical emission-line kinematics. Wilson & Baldwin (1985) find that the kinematic centre of NGC 2110, as derived from the op-

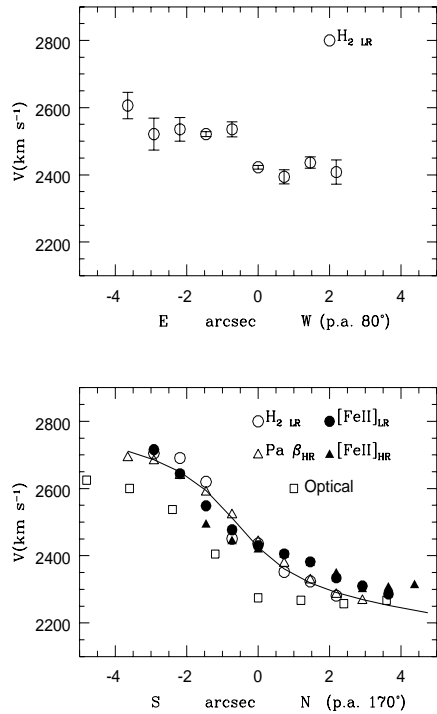


Figure 5. Heliocentric rotation curve of NGC 2110, obtained from the peak wavelengths of the emission lines. The subscripts on the labels indicate the grating used. The continuous line is the fit of a model with circular rotational motions to the $\text{Pa}\beta$ and H_2 data along $\text{p.a.} = 170^\circ$ (radio axis). For clarity, error bars have been shown only in the upper panel, but are mainly dependent on the distance to the nucleus and approximately apply also to the lower panel. The average peak velocities from $[\text{OIII}]\lambda 5007$ and $\text{H}\beta$ (Wilson & Baldwin 1985) are represented by open squares.

tical emission-line rotation curve, is displaced $1.7''$ S of the optical nucleus (identified with the peak of continuum light) along $\text{p.a.} = 161^\circ$. In order to search for any similar shifts in our data, we have fitted a model with circular rotational motions (Bertola et al. 1991) to the peak velocities of $\text{Pa}\beta$ and H_2 (omitting the the $[\text{FeII}]$ line as its motions may be affected by interactions with the radio jet) along $\text{p.a.} = 170^\circ$, allowing for a shift x_0 in the position of the kinematic centre with respect to the nucleus. This fit shows that the data are consistent with circular motions in the plane of the galaxy disk, with the kinematic centre shifted by $x_0=0.6''$ S with respect to the peak of the continuum IR light. This shift is in the same direction as that from the optical observations, but is smaller. In order to investigate this difference, we have also plotted in Fig. 5 the average of the $[\text{OIII}]$ and $\text{H}\beta$ peak velocities of Wilson and Baldwin (1985), assuming the optical and infrared nuclei coincide. The kinematic centre of this optical rotation curve is seen to be displaced $\approx 1.2''$ S relative to the kinematic centre of the IR curve.

The above results suggest that the apparent displacement between the kinematic and photometric nucleus is, at least in part, an effect of obscuration. The difference between the optical and IR rotation curves may result from either a shift between the IR and optical continuum peaks and/or the fact that the IR emission lines sample the NLR

kinematics closer to the nucleus (see discussion by Wilson & Baldwin 1985 and Wilson, Baldwin & Ulvestad 1985).

3.1.3 Emission line fluxes and ratios

Fig. 6 shows the line fluxes as a function of distance from the nucleus. In order to be able to compare the flux distributions along the the N–S and E–W directions, we have de-projected the angular distances assuming the gas lies in the plane of the stellar disk and adopting an inclination $i = 53^\circ$ and a major axis $\text{p.a.} = 160^\circ$ (Wilson & Baldwin 1985). The $[\text{FeII}]\lambda 1.257\mu\text{m}$ line fluxes obtained from the LR spectra are $\approx 30\%$ larger than that from the HR spectra, but when corrected for the different slit widths ($1.1''$ for the LR and $1.7''$ for the HR spectra), this difference increases to a factor of 2. At least part of this difference can be attributed to a somewhat poorer seeing in the second observing run.

It can be seen in the left panels of Fig. 6 that the $[\text{FeII}]$ lines are more extended to the N ($5''$) than to the S ($3''$), with a small “bump” to the N, following the radio emission. (Due to observing constraints, it was not possible to obtain a J spectrum perpendicular to the radio axis). The $\text{Pa}\beta$ flux distribution (upper right panel of Fig. 6) shows similar extent to N and S, being flatter to the S.

The H_2 flux distribution is presented in lower right panel of Fig. 6. After de-projection, there is no significant asymmetry in either the N–S or E–W H_2 flux distributions within $3''$ of the nucleus. The H_2 line is detected further from the nucleus along the E–W direction than along the N–S direction. Although a compact molecular torus may contribute to the H_2 emission, the line extends to ≈ 1 kpc from the nucleus. Moreover, the H_2 kinematics are consistent with circular motion in the disk of the galaxy (Section 3.1.2).

The luminosity in the H_2 line can be used to estimate the mass of hot molecular hydrogen in NGC 2110. We have used the method described by Veilleux et al. (1997), which is based on the calculations of Scoville et al. (1982). Adopting cylindrical symmetry for the H_2 flux distribution, we obtain an integrated $\text{H}_2 v=1-0 \text{ S}(1)$ luminosity in the inner $10''$ (Fig. 6) of $L_{\text{H}_2} = 6.7 \times 10^{39} \text{ ergs s}^{-1}$. If the hot H_2 molecules are thermalized at $T=2000 \text{ K}$, and assuming that the power in all H_2 lines is 10 times that in the $\text{S}(1)$ line, this luminosity translates into a hot H_2 mass of $2,300 \text{ M}_\odot$. If we correct the H_2 luminosity for extinction (adopting $E(\text{B}-\text{V})=1.5$ – see below) the luminosity and resulting mass would be $\approx 60\%$ larger.

The emission-line ratio $[\text{FeII}]\lambda 1.257/\text{Pa}\beta$ as a function of distance from the nucleus along the radio axis is presented in Fig. 7. It reaches very high values at the nucleus: ≈ 7 , much higher than the value of ≈ 1 found in NGC 1068, for example (Ward et al. 1987). It decreases more slowly to the N (along the radio emission) than to the S, and only in the outermost regions of NGC 2110 does this ratio approach unity.

The origin of the $[\text{FeII}]$ emission in Seyfert galaxies has been extensively discussed in previous works (e.g. Forbes & Ward 1993; Simpson et al. 1996; Veilleux et al. 1997). Possibilities include ionization by X-rays from the central source, ionization by shocks produced by interaction of a radio jet with the surrounding medium, and contributions from starbursts. However, detailed calculations by Colina

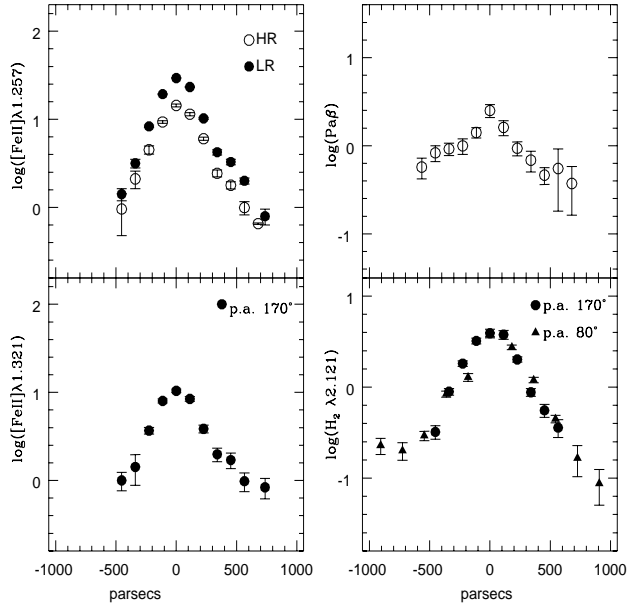


Figure 6. Logarithm of the emission-line fluxes (in units of 10^{-15} ergs $\text{cm}^{-2} \text{s}^{-1}$ (arcsec^{-2}), as a function of distance from the nucleus of NGC 2110. Circles correspond to the direction S–N (radio axis), with S negative and N positive. Triangles correspond to the direction E–W, with E negative and W positive. The x axes refer to distances in the plane of the galaxy disk (scale: 151 pc arcsec^{-1}), assuming $i = 53^\circ$ and major axis p.a.= 160° . Open symbols correspond to the HR grating, and filled symbols to the LR grating.

(1993) show that, for starbursts, $[\text{Fe II}]/\text{Pa}\beta \leq 0.4$, suggesting a starburst contribution is not important for the nuclear region of NGC 2110. Forbes & Ward (1993) favour ionization by shocks in both starbursts and Seyferts because of the correlation between $[\text{Fe II}]$ and radio fluxes, which was confirmed by the additional data of Veilleux et al. (1997). For NGC 2110 the broadening of the $[\text{Fe II}]$ profile (discussed above) at the locations where the $[\text{Fe II}]\lambda 1.257/\text{Pa}\beta$ ratio is higher, the presence of a linear radio source, and the fact that the $[\text{Fe II}]$ emission is more extended along the radio axis, give further support to this scenario. The very high nuclear $[\text{Fe II}]\lambda 1.257/\text{Pa}\beta$ ratio can thus be understood as due to the fact that while both $\text{Pa}\beta$ and $[\text{Fe II}]$ likely contain contributions from photoionization by the central source, the $[\text{Fe II}]$ emission is further enhanced by the shock ionization of Fe by the radio jet.

For the nucleus, we obtain the ratio $H_2 v=1-0 S(1)/Br\gamma \approx 3.0 \pm 2.0$; it was not possible to measure $Br\gamma$ outside the nucleus. The ratio $H_2 v=1-0 S(1)/Br\gamma$ allows us to discriminate between various excitation mechanisms for the H_2 emission. In star-forming regions, where the main heating agent is UV radiation, $H_2/Br\gamma < 1.0$, while for Seyferts this ratio is larger due to additional H_2 emission excited by shocks or by X-rays from the active nucleus (Moorwood & Oliva 1994). For NGC 2110, although some contribution from shocks cannot be discarded, the smaller width

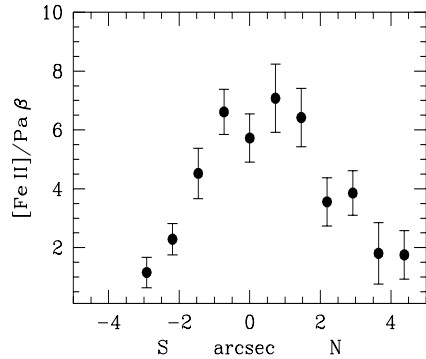


Figure 7. Emission-line ratio $[\text{Fe II}]\lambda 1.257/\text{Pa}\beta$ as a function of distance from the nucleus of NGC 2110 along the radio axis at p.a. = 170° . Negative positions are to the S and positive to N.

of the H_2 emission line when compared to that of the $[\text{Fe II}]\lambda 1.257$ suggests that the excitation of H_2 is dominated by X-rays from the active nucleus. Veilleux et al. (1997) have shown that NGC 2110 has enough X-ray emission to produce the necessary excitation.

3.1.4 Reddening and Dust Emission

The ratio between the $\text{Br}\gamma$ and $\text{Pa}\beta$ nuclear fluxes can be used to estimate the gaseous reddening at the nucleus under the assumption of Case B recombination (for $T = 10^4$ K, $\text{Br}\gamma/\text{Pa}\beta = 0.170$; Osterbrock 1989) and the reddening law from Whitford (1958) and Rieke & Lebofsky (1985), through the expression:

$$E(B-V) = 5.21 \times \log \left(\frac{F_{Br\gamma}}{F_{Pa\beta}} \right) \text{mag}$$

The resulting nuclear reddening, after subtraction of the foreground Milky Way reddening $E(B-V)_G \approx 0.36$ mag (Burstein & Heiles 1982) is $E(B-V) = 1.1 \pm 0.7$ mag. This reddening is comparable with a previous optical determination ($E(B-V) = 0.73$ mag – Shuder 1980). The error is large due to the uncertainties in the fluxes of $\text{Br}\gamma$ and $\text{Pa}\beta$ ($F_{Br\gamma} = 1.0(\pm 0.4) \times 10^{-15}$ ergs $\text{cm}^{-2}\text{s}^{-1}$; $F_{Pa\beta} = 3.0(\pm 0.4) \times 10^{-15}$ ergs $\text{cm}^{-2}\text{s}^{-1}$; both integrated over an area of $1.1'' \times 0.73''$).

The nuclear reddening can also be estimated from the slope of the continuum. We have used the spectra of Fig. 1 to obtain the J–K colours: after correcting for $E(B-V)_G$, we obtain $J-K \approx 1.9$ mag for the nucleus and ≈ 0.9 mag for the extranuclear spectra. The nuclear value is in good agreement with the colours $J-H = 0.93$ and $H-K = 1.0$ obtained by Alonso-Herrero et al. (1998) within an aperture of $1.5''$ diameter. If the intrinsic nuclear colour were the same as that of the extranuclear regions and the observed colour were a result of reddening of the starlight by dust, the nuclear obscuration is $A_V \approx 6$ mag, larger than the value obtained from the emission lines.

On the other hand, $J-K \approx 2$ is also consistent with a mixture of a late-type stellar population and emission by hot

dust (Simpson et al. 1996). In order to investigate whether obscuration or dust emission is responsible for the red nuclear colour of NGC 2110, we have compared the slopes of the nuclear continuum in our J and K band spectra with those of the extranuclear continua reddened by various values. In the J-band the slope of the nuclear continuum is very similar to that of the extranuclear continua, and is consistent with a nuclear $E(B-V) < 1.1$. But in the K-band, the continuum at the nucleus is much steeper (redder) than in the extranuclear spectra, implying $E(B-V) \geq 3$, in disagreement with the low reddening of the J-band.

We also find that extrapolation of the J-band spectrum to the K-band gives a continuum flux at $\lambda \approx 2.07\mu\text{m}$ in agreement with that observed. At longer wavelengths, the spectrum is much redder, suggesting we are seeing another component. According to models (e.g. Pier & Krolik 1993), this spectral region corresponds to the onset of the emission from a dusty torus heated by the AGN. In fact, we have successfully fitted a simple blackbody curve to the nuclear K-band spectrum, but the temperature depends on the contribution of other components, such as the underlying galaxy spectrum. For example, subtracting a constant contribution at the K-band of 85% at $\lambda 2.15\mu\text{m}$, for these components, we obtain a blackbody temperature of $T = 730$ K. We thus conclude that the red nuclear continuum is most probably a result of hot dust emission. This red continuum is only present right at the nucleus, and is not resolved (size $\lesssim 150$ pc), consistent with the torus hypothesis.

3.2 Circinus

3.2.1 Emission-line Profiles

Figure 8 shows the J and K spectra of the Circinus galaxy obtained with the HR grating along p.a. = 24° (close to the galaxy major axis), while Fig. 9 shows the spectra along p.a. = -66° (close to the radio axis). Emission in the lines $[\text{Fe II}]\lambda 1.257\mu\text{m}$, $\text{Pa} \beta$, $\text{H}_2 v=1-0$ S(1) and $\text{Br} \gamma$ extends beyond the central $15''$ covered by the slit, while the coronal line of $[\text{S IX}]$ at $\lambda 1.252\mu\text{m}$ is spatially unresolved ($\leq 1''$; 19 pc), as previously found by Oliva et al. (1994), and consistent with modelling by Binette et al. (1997).

The emission lines are barely resolved spectrally, as illustrated in Fig. 10, where the profiles of $[\text{S IX}]$, $[\text{Fe II}]\lambda 1.257\mu\text{m}$ and $\text{Pa} \beta$ in the nuclear J spectrum are shown together with the profile of a comparison lamp emission line. When corrected by the instrumental profile, the FWHM of these emission lines are 97, 143 and 133 km s^{-1} , respectively. The uncertainties are large ($30-50 \text{ km s}^{-1}$) because the uncorrected FWHM values are close to the instrumental value (150 km s^{-1}). A common characteristic of all the nuclear emission-line profiles is a slight blueward slanting asymmetry.

3.2.2 Velocity field

Figure 11 shows the heliocentric gas velocities of Circinus, obtained from the peak wavelengths of $[\text{Fe II}]\lambda 1.257\mu\text{m}$ and $\text{Pa} \beta$ along p.a. = 24° and p.a. = -66° . Also shown is the fit of a model with circular rotational motions (Bertola et al. 1991) to the data along p.a. = 24° . As in the case of

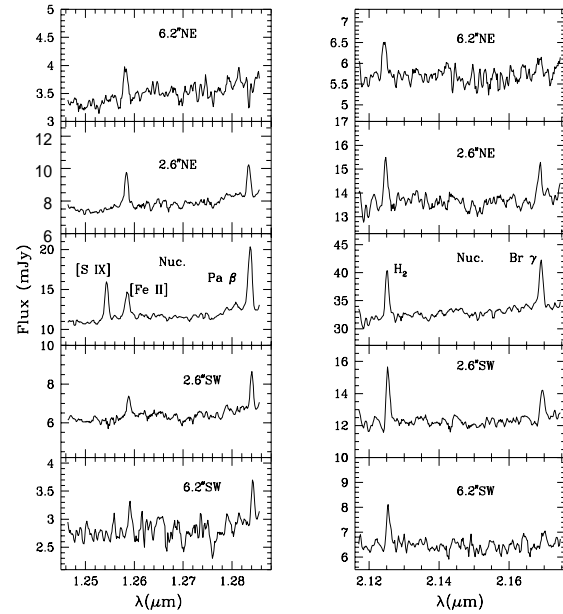


Figure 8. J and K-band spectra of Circinus at $R \approx 2000$ along the galaxy plane at $\text{p.a.} = 24^\circ$ after binning 2 pixels ($0.73''$) together. The distance from the nucleus is indicated.

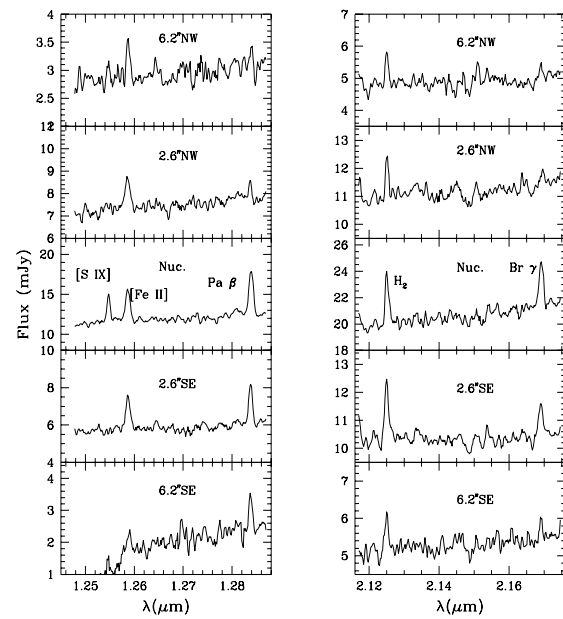


Figure 9. J and K-band spectra of Circinus at $R \approx 2000$ along the radio axis at $\text{p.a.} = -66^\circ$ after binning 2 pixels ($0.73''$) together. The distance from the nucleus is indicated.

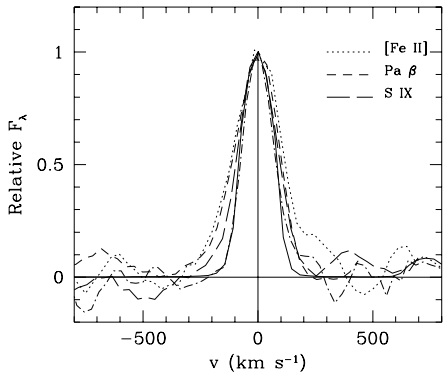


Figure 10. Comparison of the nuclear emission-line profiles of Circinus with the instrumental profile (continuous line).

NGC 2110, the velocity field is dominated by circular rotation in the plane of the galaxy, and the kinematic centre is displaced $1.0''$ SW of the peak of the IR continuum. Our data can be compared with IR and optical data from Maiolino et al. (1998), also shown in Fig. 11 as open squares: the inner 5 points correspond to stellar features in the K-band, and the outermost points to optical emission in $[\text{NII}]\lambda 6584$. Our results agree with Maiolino et al.'s, filling nicely the gaps in their data.

3.2.3 Emission line fluxes and ratios

Figure 12 shows the line fluxes as a function of distance from the nucleus, along $\text{p.a.} = 24^\circ$ (major axis) and $\text{p.a.} = -66^\circ$ (radio axis). The $[\text{Fe II}]\lambda 1.257\mu\text{m}$ emission is, on average, stronger along the radio axis than along the galaxy axis. The H_2 and $\text{Br} \gamma$ fluxes at the nucleus in the spectrum obtained along the radio axis are about 50% of the corresponding values in the spectrum obtained along the galaxy major axis, which suggests that the slit was not well centred in the K spectrum along $\text{p.a.} = -66^\circ$.

We have compared our flux distributions with the emission-line images of Davies et al. (1998, hereafter D98) in H_2 and $[\text{Fe II}]\lambda 1.64\mu\text{m}$. The latter line comes from the same upper level as $[\text{Fe II}]\lambda 1.257\mu\text{m}$ (having intrinsically 75% of its flux), and we can thus compare the two brightness distributions.

The H_2 brightness distribution of D98 shows a central peak, corresponding to a marginally resolved central source, with a steep radial profile, superimposed on extended emission with a shallower radial profile. From the lower left panel of Fig. 12, it can be seen that our H_2 fluxes present a similar behavior, showing a steeper flux distribution within $2''$ from the peak (which seems to be located $\approx 1''$ to SW and to SE of the peak in the continuum), than in the outer parts.

The $[\text{Fe II}]$ flux distribution of D98 is less centrally peaked, showing an extension to the N-NE. Our $[\text{Fe II}]\lambda 1.257\mu\text{m}$ flux distribution consistently shows a “flat-top” along $\text{p.a. } 24^\circ$. However, along the radio axis, our data is similarly extended as along $\text{p.a. } 24^\circ$, while D98 conclude that the $[\text{Fe II}]$ emission is less extended towards the cone.

The integrated $\text{H}_2 v=1-0, \text{S}(1)$ luminosity in the inner

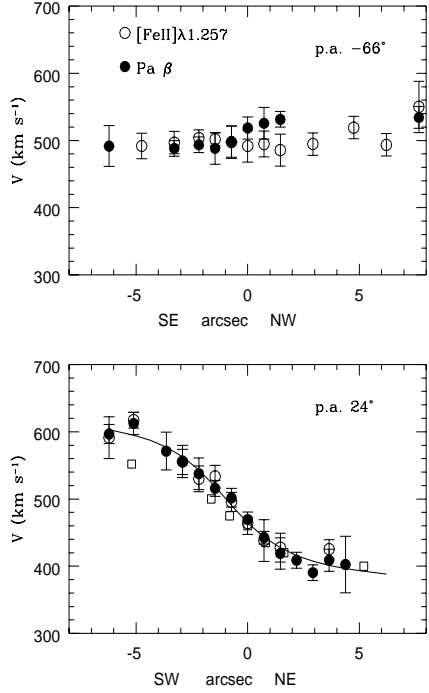


Figure 11. Rotation curve of Circinus, obtained from the peak wavelength of the emission-lines. The continuous line represents the fit of a model with circular rotational motions to the data along the galaxy plane at $\text{p.a.} = 24^\circ$. Squares represent data from Maiolino et al. (5 inner points from K-band stellar absorption features and 2 outermost points from the optical $[\text{NII}]\lambda 6584$ emission line.)

$\approx 13''$ (Fig. 12) is $4.3 \times 10^{38} \text{ ergs s}^{-1}$, which translates into a hot H_2 mass of 140 M_\odot , using the same assumptions as for NGC 2110. Allowing for an average reddening of $E(\text{B-V}) \approx 2.5$ (see below), the above luminosity and mass increase by a factor of ≈ 2.2 .

Figure 13 shows the line ratios $[\text{Fe II}]\lambda 1.257/\text{Pa} \beta$ and $\text{H}_2/\text{Br} \gamma$ along $\text{p.a.} = 24^\circ$ and $\text{p.a.} = -66^\circ$. $[\text{Fe II}]/\text{Pa} \beta$ has the value 0.4 at the nucleus and increases outwards, most notably along the radio axis, reaching values larger than 2. $\text{H}_2/\text{Br} \gamma$ presents a similar behaviour: it is ≈ 1 at the nucleus and increases outwards to values larger than 2. Both ratios at the nucleus have values typical of starbursts (see discussion above for NGC 2110), suggesting that the starburst dominates the gaseous excitation there. The larger ratios away from the nucleus suggest that X-ray radiation from the active nucleus and/or shocks dominate the excitation. In particular, the high $[\text{Fe II}]\lambda 1.257/\text{Pa} \beta$ ratios may trace the high excitation gas, which extends along the galaxy minor axis as shown by the “ionization map” (optical line ratio map $[\text{OIII}]/(\text{H}\alpha + [\text{NII}])$ of Marconi et al. (1994)).

Our results regarding the nature of the H_2 emission seem to contradict the interpretation put forward by D98. They argue that the nuclear H_2 component has the flux expected by excitation produced by the observed nuclear X-ray flux, and thus may originate from gas in the molecular torus excited by the nuclear AGN, while the more extended emis-

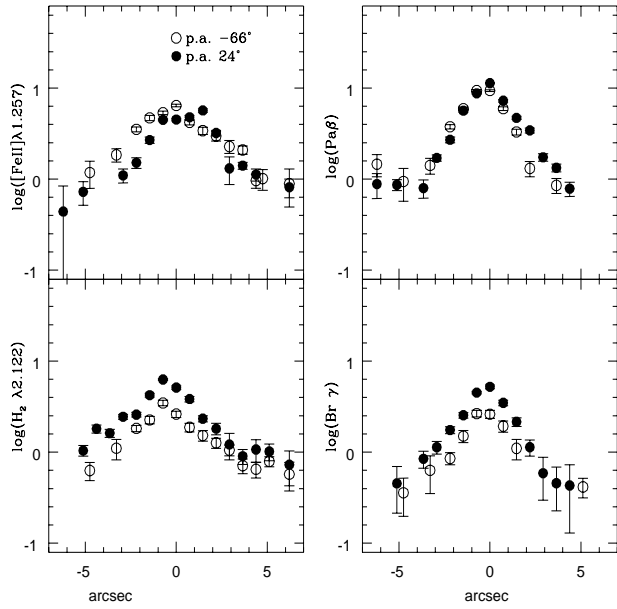


Figure 12. Logarithm of the emission-line fluxes of Circinus (in units of 10^{-15} ergs cm^{-2} s^{-1} (arcsec) $^{-2}$) as a function of distance from the nucleus, along the galaxy plane at p.a. = 24° (filled circles) and along the radio axis at p.a. = -66° (open circles). For p.a. = 24° , SW is negative and NE positive. For p.a. = -66° , SE is negative and NW positive.

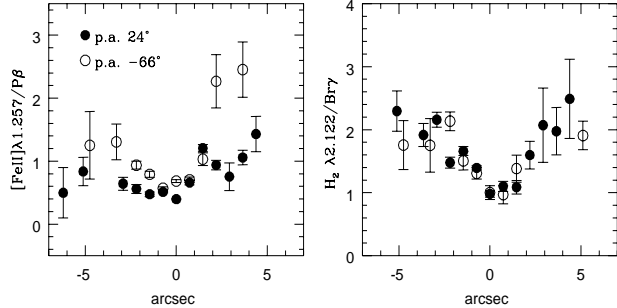


Figure 13. Emission-line ratios of Circinus as a function of distance to the nucleus along the galaxy plane at p.a. = 24° (filled circles) and along the radio axis at p.a. = -66° (open circles). Along p.a. = 24° , SW is negative and NE positive. Along p.a. = -66° , SE is negative and NW positive.

sion could be due to on-going star formation. Our results suggest the opposite is true (see Fig. 13, right panel).

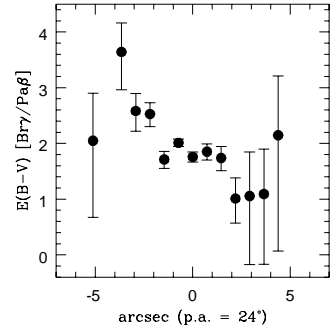


Figure 14. Reddening $E(B-V)$ (in mag) as a function of distance from the nucleus of Circinus along the galaxy plane at p.a. = 24° . SW is negative and NE positive.

3.2.4 Reddening and Dust Emission

We have used the line fluxes in $\text{Pa}\beta$ and $\text{Br}\gamma$ to obtain the gaseous reddening along p.a. = 24° (we did not calculate the reddening along p.a. = -66° due to the apparent misplacement of the slit in the K-band spectrum at this p.a.). After correction for the foreground Milky Way reddening $E(B-V)_G = 0.5$ mag (Freeman et al. 1977), the internal reddening lies in the range $1 \leq E(B-V) \leq 3.5$ mag, and increases from NE to SW, as shown in Fig. 14.

The continuum colour (corrected for $E(B-V)_G$) is reddest at the nucleus, where $J-K = 1.9$, decreasing to $J-K \approx 1.3$ to the NE, and to $J-K \approx 1.5-1.6$ to the SW.

On the assumption that the reddening derived from the emission lines can be applied to the continuum, we obtain intrinsic colours $J-K$ in the range 0.4–0.8 for the extranuclear spectra and $J-K \approx 1$ for the nuclear spectrum. The former $J-K$ colours are typical of starbursts of ages 10^6-10^8 yrs (Leitherer & Heckman 1995). This result is in agreement with the modelling of Maiolino et al. (1998), who concluded that, on the basis of a $\text{Br}\gamma$ emission map, within 100 pc from the nucleus the stellar population has an age ranging between 4×10^7 and 1.5×10^8 yrs.

4 SUMMARY AND CONCLUDING REMARKS

Long-slit spectra in the near IR J and K-bands of the Seyfert 2 galaxies NGC 2110 and Circinus have revealed extended emission in $[\text{FeII}]\lambda 1.257\mu\text{m}$, $\text{Pa}\beta$ and $\text{H}_2 v=1-0 \text{ S}(1)$ up to at least ≈ 900 pc (6'') from the nucleus in NGC 2110 and beyond the end of the slit – 130 pc (7'') from the nucleus – in the case of Circinus.

The profiles of the emission lines $[\text{FeII}]\lambda 1.257\mu\text{m}$ and $\text{Pa}\beta$ from the nucleus of NGC 2110 are broad ($\text{FWHM} \approx 500 \text{ km s}^{-1}$) and quite similar, while the profile of $\text{H}_2 v=1-0 \text{ S}(1)$ is narrower, with $\text{FWHM} \leq 300 \text{ km s}^{-1}$, and thus originates in a kinematically less disturbed gas. We do not confirm previous reports of a very broad $\text{Pa}\beta$ component. In Circinus, the profiles are barely resolved spectrally, with $\text{FWHM} \leq 150 \text{ km s}^{-1}$.

The H_2 line luminosities and masses of hot molecular gas are similar to those of other Seyfert galaxies (e.g. Veilleux et al. 1997). The $[\text{FeII}]\lambda 1.257\mu\text{m}$ emission may trace the high excitation gas. In the case of NGC 2110,

the high $[\text{Fe II}]\lambda 1.257\mu\text{m}/\text{Pa } \beta$ flux ratio combined with the broadening of the nuclear profiles suggests that shocks (perhaps driven by the radio jet) are an important source of excitation of the $[\text{Fe II}]$ emission. The high $\text{H}_2 v=1-0 \text{ S(1)}/\text{Br } \gamma$ nuclear ratio, combined with the smaller width of the H_2 emission-line, suggests that the excitation of the H_2 line is dominated by X-ray emission from the active nucleus. In the case of Circinus, the much lower ratios at the nucleus are similar to those observed for starbursts, suggesting that the nuclear starburst is the main source of excitation there. However, a few arcseconds from the nucleus, these ratios increase to values similar to those found in Seyfert nuclei, showing that the radiation of the active nucleus may be the main source of excitation outside the nucleus.

We were able to obtain rotation curves in the IR lines for both galaxies, which indicate that the gaseous kinematics are dominated by circular motions in the disks of the galaxies. In both cases we found a displacement between the peak of the IR continuum and the kinematic center of the galaxy along the p.a. closest to the major axis. In the case of NGC 2110, this effect had been previously found using optical observations, but the IR rotation curve is more symmetric relative to the nucleus than the rotation curve obtained from optical lines. This result suggests that the offset of the continuum nucleus with respect to the kinematic centre is, at least in part, an effect of obscuration.

For NGC 2110, $J-K \approx 0.9$ everywhere, except right at the nucleus, where $J-K \approx 1.9$. The continuum spectrum within the K band is very steep and cannot be explained by reddening alone. The observations clearly show that we are seeing another component in emission in the K-band, which is consistent with the expected emission of dust heated by an AGN. This emission is unresolved in our data ($0.73'' \times 1.1''$), and may originate in the walls of a circumnuclear dusty torus.

For Circinus, the $\text{Br } \gamma/\text{Pa } \beta$ ratios indicate gaseous reddening in the range $1 \leq E(B-V) \leq 3$. The $J-K$ values are consistent with those of an ageing starburst with the same reddening as the emitting gas, except at the unresolved nucleus, which has a redder colour.

ACKNOWLEDGEMENTS

We thank the support of the staff of CTIO by assistance with the near-IR observations and reductions, in particular Richard Elston. We also thank the referee, Chris Done, for several suggestions which helped to improve the paper. This work was partially supported by the Brazilian institutions CNPq, FAPERGS and FINEP. This research has made use of the NASA/IPAC Extragalactic Database (NED), which is operated by the Jet Propulsion Laboratory, under contract with NASA.

REFERENCES

Alonso-Herrero, A., Ward, M. J. & Kotilainen, J. K. 1996, MNRAS, 278, 902
 Alonso-Herrero, A., Simpson, C., Ward, M. J. & Wilson, A. S. 1998, ApJ, 495, 196
 Antonucci, R. R. J. 1993, ARAA, 31, 473
 Antonucci, R. R. J. & Miller, J. S. 1995, ApJ, 297, 621
 Bertola, F., Bettoni, D., Danziger, J., Sadler, E., Sparke, L. & de Zeeuw, T. 1991, ApJ, 373, 369
 Binette, L., Wilson, A. S., Raga, A. & Storchi-Bergmann, T. 1997, A&a, 327, 909
 Blaetz, M., Cameron, M., Drapatz, S., Genzel, R., Krabbe, A., van der Werf, P., Sternberg, A. & Ward, M. 1994, ApJ, 421, 92
 Bradt, H. V., Burke, B. F., Canizares, C. R., Greenfield, P. S., Kelly, R. L., McClintock, J. E., Van Paradijs, J. & Koski, A. T. 1978, ApJ, 226, L111
 Burstein, D. & Heiles, C. 1982, AJ, 87, 1165
 Cid Fernandes, R., Storchi-Bergmann, T. & Schmitt, H. R. 1998, 297, 259
 Colina, L. 1993, ApJ, 411, 565
 Davies, R. I., Forbes, D. A., Ryder, S., Ashley, M. C. B., Burton, M., Storey, J. W. V., Allen, L. E., Ward, M. J. & Norris, R. P. 1998, MNRAS, 293, 189
 Elias, J. H., Frogel, J. A., Matthews, K. & Neugebauer, G. 1982, AJ 87, 1029.
 Elmoutie, M., Haynes, R. F., Jones, K. L., Ehle, M., Beck, R. & Wielebinski, R. 1995, MNRAS 275, L53
 Forbes, D. A. & Ward, M. J. 1993, ApJ, 416, 150
 Freeman, K. C., Karlsson, B., Lynga, G., Burrell, J. F., van Woerden, H., Goss, W. M. & Mebold, U. 1977, A&A, 55, 445
 Glass, I. S. & Moorwood, A. F. M. 1985, MNRAS, 214, 429
 Leitherer, C. & Heckman, T. M. 1995, ApJS, 96, 9
 Maiolino, R., Krabbe, A., Thatte, N. & Genzel, R. 1998, ApJ, 493, 650
 Marconi, A., Moorwood, A. F., Origlia, L., Oliva, E. 1994, ESO Messenger, No. 78, 20
 McAlary, C. W. & Rieke, G. H. 1988, ApJ, 333, 1
 Moorwood, A. F. M. & Oliva, E. 1988, A&A, 203, 278
 Moorwood, A. F. M. & Oliva, E. 1990, A&A, 239, 78
 Moorwood, A. F. M. & Oliva, E. 1994, ApJ, 429, 602
 Moorwood, A. F. M., van der Werf, P. P., Kotilainen, J. K., Marconi, A. & Oliva, E. 1996, A&A, 308, 1
 Mulchaey, J. S., Wilson, A. S., Bower, G. A., Heckman, T. M., Krolik, J. H. & Miley, G. K. 1994, ApJ, 433, 625
 Mulchaey, J. S., Wilson, A. S. & Tsvetanov, Z. I. 1996, ApJS, 102, 309
 Oliva, E., Salvati, M., Moorwood, A. F. M. & Marconi, A. 1994, A&A, 288, 457
 Osterbrock, D. E. 1989, *Astrophysics of Gaseous Nebula and Active Galactic Nuclei*, University Science Books, Mill Valley, California
 Pier, E. A. & Krolik, J. H. 1993, ApJ, 418, 673
 Puxley, P. J., Lumsden, S. L., Brand, P. W. J. L. & Doyon, R. 1994, MNRAS, 270, L7
 Rieke, G. H. & Lebofsky, M. J. 1985, ApJ, 288, 618
 Sanders, D. B., Phinney, E. S., Neugebauer, G., Soifer, B. T., Matthews, K., 1989, ApJ, 347, 29
 Scoville, N. Z., Hall, D. N. B., Kleinmann, S. G. & Ridgway, S. T. 1982, ApJ, 253, 136
 Shuder, J. M. 1980, ApJ, 240, 32
 Simpson, C., Forbes, D. A., Baker, A. C. & Ward, M. J. 1996, MNRAS, 283, 777
 Simpson, C., Mulchaey, J. S., Wilson, A. S., Ward, M. J. & Alonso-Herrero, A. 1996, ApJ, 457, L19
 Storchi-Bergmann, T., Wilson, A. S. & Baldwin, J. A. 1992, ApJ, 396, 45
 Storchi-Bergmann, T., Wilson, A. S. & Baldwin, J. A. 1996, ApJ, 460, 252
 Storchi-Bergmann, T., Kinney, A. L. & Challis, P. 1995, ApJS, 98, 103
 Ulvestad, J. S. & Wilson, A. S. 1983, ApJ, 264, L7
 Veilleux, S., Goodrich, R. W. & Hill, G. J. 1997, ApJ, 477, 631
 Ward et al. 1987, ApJ, 316, 138
 Whitford, A. E. 1958, AJ, 63, 201

Wilson, A. S. & Baldwin, J. A. 1985, ApJ, 289, 124
Wilson, A. S., Baldwin, J. A. & Ulvestad, J. S. 1985, ApJ, 291,
627